# 3
# Localized Light-Matter Interactions with Optical Antennas

**Zachary J. Lapin, Palash Bharadwaj, Shawn Divitt, and Lukas Novotny**

**Abstract** Standard far-field optical elements, such as lenses and mirrors, are only capable of localizing radiation to about half-a-wavelength—the Abbe criterion. Optical antennas facilitate the further localization of radiation into arbitrarily small spatial volumes. Combining the optical antenna with traditional optical microscopy, a technique termed near-field scanning optical microscopy (NSOM), has enabled the study of biological and solid-state samples at high spatial resolution. Since the development of NSOM in the 1980s, the biggest challenge to researchers has been the design and fabrication of optical antennas functioning as optical near-field probes. We have recently made much progress in the development of widely applicable, and reproducible, optical antennas that provide a high degree of spatial localization. Beyond NSOM, we also explore the electrical excitation, as opposed to photo excitation, of optical antennas with a scanning tunneling microscope (STM). We demonstrate a two-step plasmon-mediated energy conversion from a tunneling current to propagating photons in a smooth gold film as well an extended gold nanowire. We prove that highly localized gap plasmons are first excited in the tunnel gap, which can then couple to propagating plasmons. We elaborate on the role of gap plasmons in explaining the huge variations seen in photon emission yields in the field of STM light emission.

**Keywords** Optical antenna • Near-field microscopy • NSOM • STM light emission

Z.J. Lapin (✉) • P. Bharadwaj • S. Divitt • L. Novotny
ETH Zürich, Zürich, Switzerland
e-mail: zlapin@ethz.ch; palashb@ethz.ch; sdivitt@ethz.ch; lnovotny@ethz.ch

B. Di Bartolo et al. (eds.), *Nano-Structures for Optics and Photonics*,
NATO Science for Peace and Security Series B: Physics and Biophysics,
DOI 10.1007/978-94-017-9133-5_3, © Springer Science+Business Media Dordrecht 2015

## 3.1 Introduction

The need for optical antennas is motivated by the diffraction limit. Standard optical microscopy and spectroscopy rely entirely on far-field optical elements such as lenses and mirrors. These elements limit the obtainable localization of radiation to about half-a-wavelength—the Abbe criterion [1, 2]. The extreme localization of incident radiation afforded by an antenna, as has been well studied at radio and microwave frequencies, is limited only by the antenna geometry. Using our previous definition of an optical antenna as *a device designed to efficiently convert free-propagating optical radiation to localized energy, and vice versa* [3], we find there to be a broad range of applications of the optical antenna in both fundamental research and engineering.

Imaging and spectroscopy at optical frequencies with sub-diffraction spatial resolution, termed near-field scanning optical microscopy (NSOM), has been demonstrated as a robust tool for understanding both physical and biological systems. While there are competing NSOM technologies, the use of the optical antenna has proven to be the most versatile. Applications include single molecule spectroscopy [4], nanoplasmonics [5, 6], biological protein mapping [7–9], fluorescence photophysics [10, 11], Raman spectroscopy [11–14], non-linear optics [15], Green's function measurements [16], interferometry [17, 18], absorption spectroscopy [19], and others.

The broad applicability of the optical antenna is made even more impressive given the infancy of the technology. The history of the optical antenna, specifically the first proposal of accessing optical near-fields, began in 1928 with a prophetic letter to Albert Einstein by a relatively unknown Edward Hutchinson Synge [20]. Synge made two separate suggestions, one relying on localized optical near-fields leaking out of a sub-wavelength aperture (the aperture probe) and the other relying on a single metallic nanoparticle that would be employed to localize and scatter optical near-fields. These ideas, however, were well ahead of the times and are in fact the first proposal of scanning microscopy techniques [21]. Both of Synge's ideas would be realized soon after the development of scanning probe microscopy (SPM) technology.

In general, the extreme localization of radiation afforded by the optical antenna facilitates the study of biological and solid-state systems in two distinct manners—spatial and optical. Spatially, the antenna facilitates resolving features that are separated by sub-diffraction length scales that are therefore simply not resolvable with traditional far-field optical techniques.

## 3.2 NSOM Imaging with Optical Antennas

The development of near-field optical techniques and the application of optical antennas has a rich history. Many technological advances were required before Synge's 1928 ideas could be experimentally realized. There are several review

articles that cover all of the developments of NSOM [20, 22]. Here, advancements that were required to achieve the imaging and spectroscopic technology that is used today will be briefly outlined.

The first necessary advancement came in the 1980s with the development of SPM. First achieved with scanning tunneling microscopy (STM) in 1982 by researchers at IBM in Switzerland [23, 24], SPM techniques allow for sub-nanometer distance control between a probe and a sample of interest. The development of the atomic force microscope (AFM) quickly followed, allowing for the fine distance control between nearly any probe and sample (not just conducting samples and probes as in STM), as well as increasing the probe-sample distance relative to STM (a feature necessary for fluorescence imaging and spectroscopy) [25].

With this technology at hand, the first near-field optical measurements were made on October 22, 1982 by Winfried Denk working with Dieter Pohl at IBM using an aperture probe [20]. Pohl published his first near-field images in 1984 [26]. The technique, termed the "optical stethoscope", a corollary to the medical stethoscope, achieved $\lambda/20$ resolution with a $\lambda = 488$ nm excitation.

Scattering-type NSOM (sometimes referred to as s-NSOM, herein referred to as NSOM) and imaging based on plasmonic resonances was published a few years later by Ulrich Ch. Fischer and Pohl [27]. Their experiment was the first realization of Synge's proposed metallic point scatterer optical antenna. In fact, any near-field probe can be viewed as an antenna since it exploits a near-field interaction for the localization of optical radiation. A further development in NSOM was the use of a sharp tungsten wire as the near-field probe [5]. This type of probe geometry has proved to be a very good optical antenna for many applications.

Today, the biggest remaining challenge for optical antennas as a near-field optical probe is the design and fabrication of the antenna itself. Despite analogies between radio/microwave and optical antennas, which are both described by the same antenna parameters, the realization of the two categories of antennas are quite different. Specifically, standard antenna designs do not always scale well into the optical regime. There are two primary reasons for this: (1) metals behave as strongly coupled plasmas at optical frequencies [28] and (2) the absolute fabrication tolerances of optical antennas is extremely difficult to achieve due to their small physical size. In fact, the motivation to study localized light-matter interactions with optical antennas has helped fuel the development of novel nanofabrication technologies.

### *3.2.1 Experimental Setup*

Most applications of SPM with optical antennas are done in transmission, with an experimental setup representatively shown in Fig. 3.1. In our experiments, an optical excitation is provided by a tightly-focused radially polarized laser source. The excitation is further localized by an optical antenna positioned above the sample and centered in the optical focus. The optical antenna-sample separation

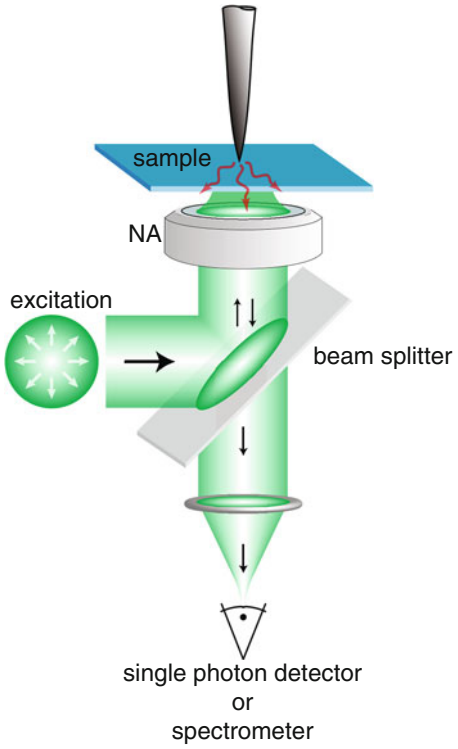


**Fig. 3.1** Schematic diagram of the experimental setup used for both NSOM and STM-LE. For NSOM, a radially polarized optical excitation is focused onto the sample by a high-NA objective. Light is further localized by the optical antenna. Spectroscopic emission is collected by the same objective and sent to either a spectrometer or single photon detector. For STM-LE, a bias is placed between the optical antenna and sample and no optical excitation is used. The sample is then raster-scanned between the optical antenna and the objective to form an image

can be maintained with either AFM or STM feedback. Spectroscopic signal from the sample is collected by the objective and sent to either a photodetector or spectrometer. Images are formed by raster-scanning the sample between the tip and focus. The system can easily be modified for STM-based light emission (STM-LE) by simply removing the optical excitation and using an STM feedback loop.

### *3.2.2 Optical Antenna Geometries*

Perhaps the most difficult challenge in optical antenna based microscopy is finding an antenna that works well for a single application, let alone a universal antenna geometry. Due to limitations in nanofabrication technologies, it has been a challenge to develop reproducible optical antennas that provide large localized field enhancements and do not quench the signal that is generated by the sample.

In NSOM, as shown in Fig. 3.1, a relatively large area of the sample is illuminated by standard, diffraction-limited, far-field optics. The optical antenna then performs two functions: a local excitation source and a local scatterer. This type of illumination scheme will lead to a detected optical signal that is a superposition of optical signals generated from the far-field excitation (termed background) and the optical

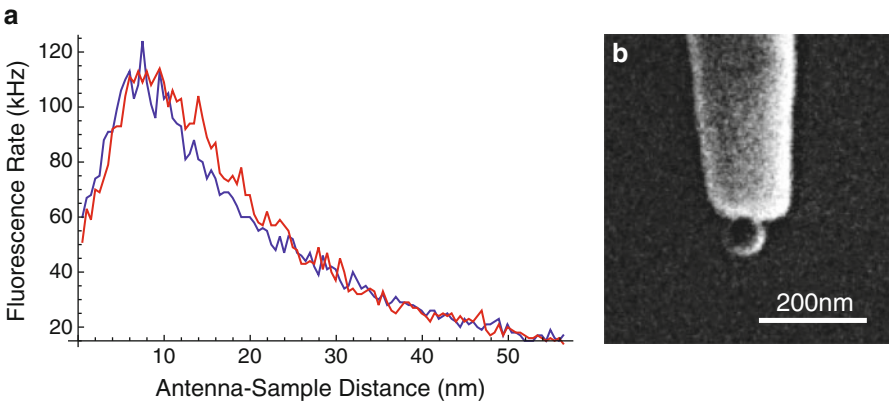


**Fig. 3.2** (**a**) An approach curve showing the fluorescence rate enhancement of a single Nile Blue molecule on cover glass as a function of the antenna-sample separation and (**b**) an electron micrograph of a representative particle antenna

antenna. The background is undesirable, however, with the combination of a good antenna, the appropriate sample, and optional real-time background suppression techniques, this methodology is extremely robust.

In general, the optical antenna facilitates the transfer of energy between the near-field and far-field equally well in both directions; however, the proximity of the antenna to the sample can also suppress the signal generated by the sample, for example, it can alter the quantum efficiency (QE) of a fluorescent molecule [11]. In the absence of the antenna (free space), the fluorescence rate of a single molecule excited below saturation, $\Gamma_{\mathrm{fl}}^{\circ}$, is the product of the excitation rate, $\Gamma_{\mathrm{exc}}^{\circ}$, and the intrinsic QE, $Q_i$, of the molecule,

$$\Gamma_{\mathrm{fl}}^{\circ} = \Gamma_{\mathrm{exc}}^{\circ} \cdot Q_i = \Gamma_{\mathrm{exc}}^{\circ} \cdot \frac{\Gamma_{\mathrm{rad}}^{\circ}}{\Gamma_{\mathrm{rad}}^{\circ} + \Gamma_{\mathrm{nr}}^{\circ}}, \tag{3.1}$$

where, subscripts "rad" and "nr" refer to the radiative and non-radiative decay processes. Coupling a fluorescent molecule, excited below saturation, to an optical antenna will alter both the excitation rate and the QE of the molecule. The increase in the excitation rate will result in an increased radiative rate (enhancement), while the presence of the metallic antenna will also affect the decay rates. Large increases in QE for molecules with a low $Q_i$ have been demonstrated [11].

#### 3.2.2.1 Metallic Particle Antennas

The first optical antenna described as well as the first used was a simple metallic sphere, now referred to as the particle antenna (cf. Fig. 3.2). The metallic nanopar-

ticle is suspended by a dielectric and functions as a dipole resonator to localize an incident optical excitation. Despite the non-optimized spherical geometry, the particle antenna does have several advantages over other antenna geometries. The colloidal synthesis of metallic nanoparticles makes it quite simple to reproducibly fabricate antennas. Additionally, the well defined spherical geometry is relatively easy to simulate and understand [29].

The most important parameters regarding a metallic nanosphere as an optical antenna are the particle's scattering cross-section,

$$\sigma_{scatt} = \frac{k^4}{6\pi\epsilon_0^2}|\alpha(\omega)|^2, \tag{3.2}$$

and the particle's absorption cross-section,

$$\sigma_{abs} = \frac{k}{\epsilon_0}\Im[\alpha(\omega)]. \tag{3.3}$$

Here, $k = \sqrt{\epsilon_d}w/c$ is the wave vector in the surrounding medium and $\alpha(\omega)$ is the quasi-static polarizability of the particle. Since $\alpha(\omega) \propto R^3$, for small particles it can be seen that the particle's absorption cross-section will be larger than the scattering cross-section. While small particles lead to strong absorption, large particles provide poor localization. We have found that an 80 nm diameter gold particle provides a good compromise between absorption and localization.

The 80 nm diameter gold particle antenna provides a 10-fold increase in the fluorescence emission rate of a high-QE single fluorescent emitter excited below saturation—both theoretically and experimentally. Figure 3.2a shows the enhancement of the collected fluorescence emission rate of a single high-QE fluorescent molecule as a function of the particle-molecule separation for a particle antenna shown in Fig. 3.2b. The emission rate is enhanced 10-fold at the optimum antenna-sample separation followed by a net fluorescence quenching as the separation is further decreased. This quenching is due to additional pathways for the excited molecule to non-radiatively transfer energy into the gold particle. The approach curve also shows that the localized field extends ~40 nm below the particle. In addition to the fluorescence-rate enhancement, a localization of radiation in the sample-plane of ~60 nm is measured for an 80 nm gold particle (Fig. 3.3a). This is well below the diffraction-limit for the red light ($\lambda = 632.8$ nm) used in this measurement.

We have also extended this imaging system to quantitative biological measurements [9]. Biological measurements impose additional challenges since biological entities are not isolated but instead exist in an optically active matrix. In order to have high quality imaging with a sufficient signal-to-background ratio, a real-time background suppression technique has been employed. This is achieved by modulating the antenna-sample separation, thereby modulating the fluorescence signal, and then demodulating the detected fluorescence signal [8]. In this way, it is possible to isolate when a fluorescent molecule is directly below the antenna

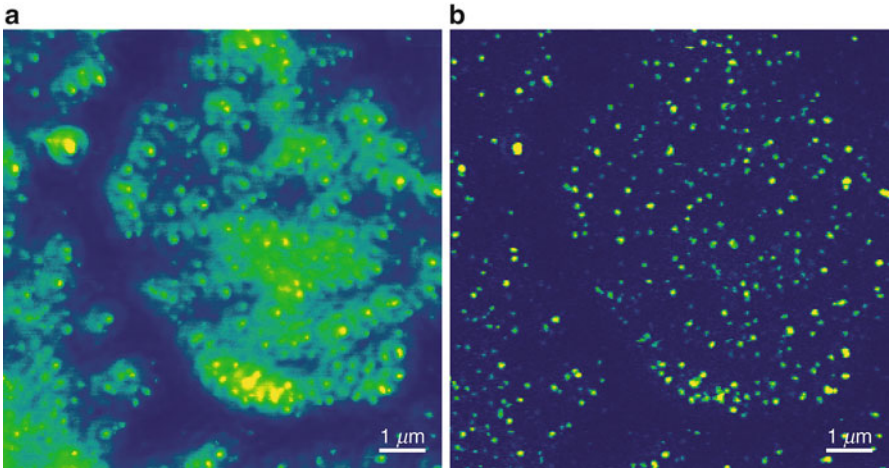


**Fig. 3.3** A comparison between an NSOM image (**a**) and a simultaneously acquired background suppressed NSOM image (**b**). The sample is a human erythrocyte ghost on a glass substrate that is labeled against the membrane protein Complement Receptor 1

and successfully suppress all background optical signal arising from the biological matrix. Figure 3.3 shows a comparison between simultaneously acquired NSOM and background suppressed NSOM images of a human erythrocyte membrane ghost labeled against Complement Receptor 1.

The single particle antenna is limited by two competing requirements: large field enhancement and high spatial confinement. These two concerns can be simultaneously satisfied by the self-similar particle antenna. An antenna comprised of a linear chain of particles of decreasing diameter has demonstrated large improvements in both enhancement and resolution for applications in fluorescence imaging and spectroscopy [30].

#### 3.2.2.2 Pyramidal Optical Antennas

The search for a more-ideal optical antenna for fluorescence imaging, meaning improved antenna performance, ease of fabrication, and reproducibility, has lead to the pyramid antenna. The antennas, formed by template-stripping metallic structures from an anisotropically etched silicon wafer, are pyramidal in shape with a tip apex on the order of 10 nm and a cone angle of 70.52°. Such a probe is capable of the localization of optical radiation exceeding that of a gold particle. Additionally, the large cone angle of the pyramid provides a large mode mismatch between radiation emitted by the sample of interest and plasmons propagating along the pyramid, thus limiting fluorescence quenching. Because of this fact, these optical antennas have been shown to have applications in both fluorescence and Raman spectroscopy and imaging [14].

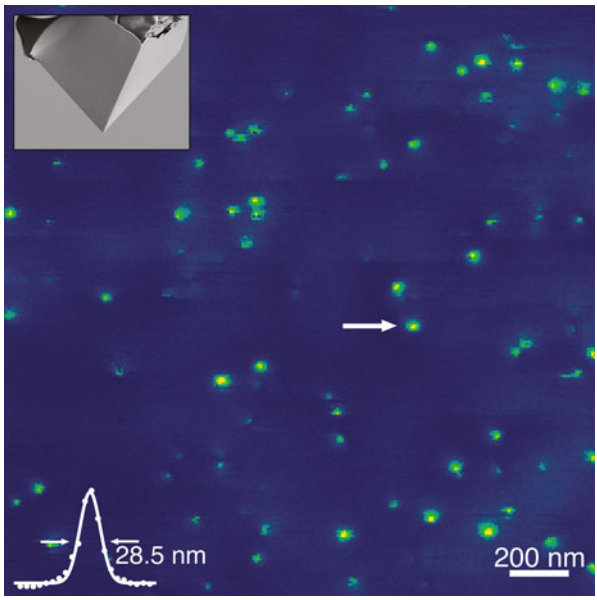


**Fig. 3.4** An NSOM image of single Atto 647N dye molecules dispersed on a ∼2 nm thick layer of PMMA on coverglass. A cross-section of a single molecule oriented perpendicular to the surface is shown. The *inset* is an electron micrograph of a representative gold pyramid antenna with a 20 μm base

The pyramid antenna has demonstrated single fluorescent molecule imaging with both resolution and enhancement exceeding that of a particle antenna. An approach curve for an isolated molecule oriented along the axis of the antenna maps the localization of radiation of the antenna to ∼15 nm and reveals a fluorescence enhancement of 200-fold [14]. Shown in Fig. 3.4, high-resolution imaging of single fluorescent molecules can easily be achieved with the pyramidal antenna geometry. Analogous to the gold particle antenna, the orientation of the molecule's absorption dipole is imaged due to the known excitation polarization [10].

The fluorescence enhancement provided by the pyramid antenna is a complex mixture of the local field enhancement, quenching, and a redirection of fluorescence emission. The Raman enhancement of a single carbon nanotube (CNT) is able to more accurately demonstrate the local field enhancement as Raman is not quenched and the redirection of optical emission can at most enhance the collected spectroscopic signal by a factor of 2. Figure 3.5 shows the Raman spectrum of a CNT. After accounting for the 1-dimensional nature of the CNT and the 0-dimensional localization of optical radiation from the antenna, an electric field enhancement of 7.5 has been demonstrated.

#### 3.2.2.3 Sharp Metallic Optical Antennas

As mentioned previously, the sharp metallic probe has proven to be a very effective optical antenna for many applications. With a relatively simple fabrication process of electrochemically etching a thin metallic wire, high resolution optical antennas with large local electric field enhancements have been realized by many

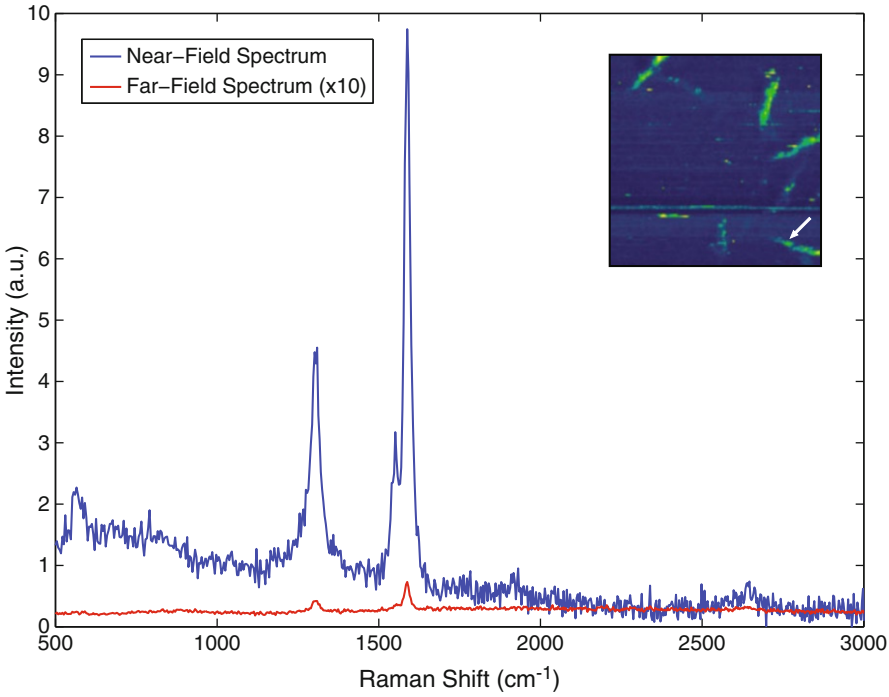


**Fig. 3.5** A TERS spectrum of a single CNT acquired with a gold pyramid antenna and the corresponding far-field spectrum. The gold pyramid antenna provides a local electric field enhancement of 7.5. The *inset* shows a $1.5 \times 1.5\,\mu m^2$ area TERS G-band image of the CNTs with the spectrum acquired at the *white arrow*. The far-field spectrum is enhanced 10-fold for visibility

research groups. Little experimental control exists, however, over the exact antenna geometry and crystal structure. This has limited the reproducibility of antennas and additionally makes the exact simulation of antenna behavior impossible.

Despite these challenges, we performed the first simulations of the enhanced electric field at the apex of an ideal sharp metallic probe in 1997 [31]. The results revealed that there can be an electric field enhancement at the tip of a sharp metallic probe if the polarization of the optical illumination is parallel to the axis of the probe. The simulations showed an electric field enhancement of 3,000 for a gold tip surrounded by water. Additionally, in the following year, we also published simulations using a tightly focused $HG_{10}$ laser mode to create a longitudinal polarization at the focus in conjunction with a sharp metallic probe [32].

While these antennas provide a significantly enhanced local electric field at the tip apex, they are generally not well suited for fluorescence measurements. This is due to the extended antenna geometry and small cone angle that allows for a fluorescent molecule in its excited state to efficiently non-radiatively transfer energy into a propagating surface plasmon along the antenna shaft, leading to quenching. For applications in Raman spectroscopy and imaging, however, the inherently low QE

and scattering cross-section means that despite the introduction of additional non-radiative decay pathways, the large local field enhancement of the optical antenna results in net emission enhancement and has achieved some of the highest spatial resolution optical images [13].

### *3.2.3 Concluding Remarks on NSOM*

The use of optical antennas for applications in microscopy and spectroscopy has made nanometer spatial resolution imaging possible on many optically active systems. The NSOM community has been rapidly expanding with the commercial development of practical NSOM systems, enabling the study of an increasing variety of samples by experts in their respective fields. Despite this progress, however, it is important to note that challenges still remain. The task of developing the most ideal antenna may end with the template-stripped pyramid antenna but other issues remain. Specifically, the spectroscopic community is concerned with precisely how each individual antenna alters the measured spectroscopic signal of a control sample. The current momentum in the field will insure that these questions, and others, are answered and that the optical antenna will continue to play an increasingly prominent role in microscopy and spectroscopy.

## 3.3 Towards Electrically Excited Optical Antennas

So far we have considered optical antennas as devices that transduce between propagating and localized fields. On the one hand, a receiving optical antenna takes far-field radiation from a laser and concentrates it into a subwavelength volume. On the other, a transmitting antenna is fed by the near-field of radiating molecules and nanotubes. This 'light-in light-out' modality is different from a typical radio/microwave antenna which is fed by an oscillating electric current at the feedgap. In this section we move away from the theme of antenna-emitter interactions and instead explore the possibility of exciting optical antennas electrically. As will be seen below, it is not necessary to impress an alternating current at optical frequencies to achieve this, rather the discreteness of a direct current across a tunnel junction suffices to create the required optical field oscillations.

### *3.3.1 Excitation of Surface Plasmons in an STM*

Since metallic optical antennas can be seen as leaky resonators for localized surface plasmons (LSPs), a more fundamental question to ask is whether surface plasmons can be excited using electrons. It has been known since the 1960s that high energy electrons impinging on metals can excite both bulk and surface plasmons [33, 34].

With the resurgence of interest in surface plasmons in recent years, there has been a revival of interest in the use of energetic (∼30 keV) electron beams to excite propagating [35–37] as well as LSP modes in metal films and nanostructures [38,39]. In a remarkable breakthrough in 1976, Lambe and McCarthy found a fundamentally new way to generate light using inelastic electron tunneling in experiments with metal-insulator-metal (MIM) junctions [40]. The role of surface plasmons as intermediaries in the inelastic process was suspected, if not proven, by these authors. The same phenomenon was rediscovered in a different context with the observation of light emission from the tunnel junction of an STM in the late 1980s [41,42]. It was hypothesized that STM-LE originates from the radiative decay of highly localized gap plasmons from the tip-sample cavity. The gap plasmons, excited by inelastically tunneling electrons, were proposed to behave as a dipole source oriented along the electron tunneling axis [43, 44]. It was further suggested that gap plasmons could also couple to propagating surface plasmon polaritons (SPPs) which could then scatter into photons [45, 46]. At this point, neither the existence of the dipolar gap plasmon nor the coupling to SPPs had been conclusively proven.

We have studied STM-LE in ambient conditions with high-NA light collection (Fig. 3.1) to help answer some of these questions [47]. Initial experiments investigated the electrical excitation of propagating plasmons on a 20 nm thick thermally evaporated gold film on a glass substrate (n = 1.52). In a typical experiment, a chemically etched gold tip (diameter ≈ 50 nm) was used to tunnel electrons into the film (typical substrate bias $V_t = 2$ V; tunneling current $I_t = 1$ nA; tip-sample distance ∼9 Å), and any photons generated were detected with a single photon detector. Consistent with previous studies, it was found that the tunneling electrons did indeed lead to the emission of photons with an emission spectrum peaked around $\lambda = 700$ nm. The origin of the emitted photons remained unclear and could be attributed to either: (1) the direct result of the radiative decay of gap plasmons, or (2) the result of the leakage and subsequent decay of propagating gold-air SPPs into the high-index glass substrate.

In order to identify the origin of the detected photons, we measured their angular radiation pattern by imaging the back focal (Fourier) plane of the objective on to a charge coupled device (CCD) camera. The signature of SPPs is the outcoupling of photons at an angle that conserves the in-plane momentum between SPPs and photons. A free space wavelength of $\lambda = 700$ nm, corresponding to an SPP wavevector of $k_{spp} = 1.06\,k_o$, where $k_o = 2\pi/\lambda$ is the free space wavevector, gives the Kretchmann angle of $\theta_K = arcsin[1.06/1.52] = 43.8°$. As seen in Fig. 3.6, more than 80 % of the photons are indeed emitted around this so-called Kretchmann angle, and hence arise from the decay of SPPs. When the same measurement was repeated on a ∼5 nm thick gold film, which is too lossy to support an SPP, the ring at the Kretchmann angle disappeared, validating our previous conclusions.

While the above experiments on extended films offer indirect evidence of SPP excitation, it would be valuable to observe SPP scattering more directly. Towards this goal, we repeated similar measurements on micron-sized, colloidally synthesized, monocrystalline gold flakes dispersed on an indium tin oxide (ITO) coated glass substrate. The flakes were triangular in shape, ∼50 nm thick, with well-

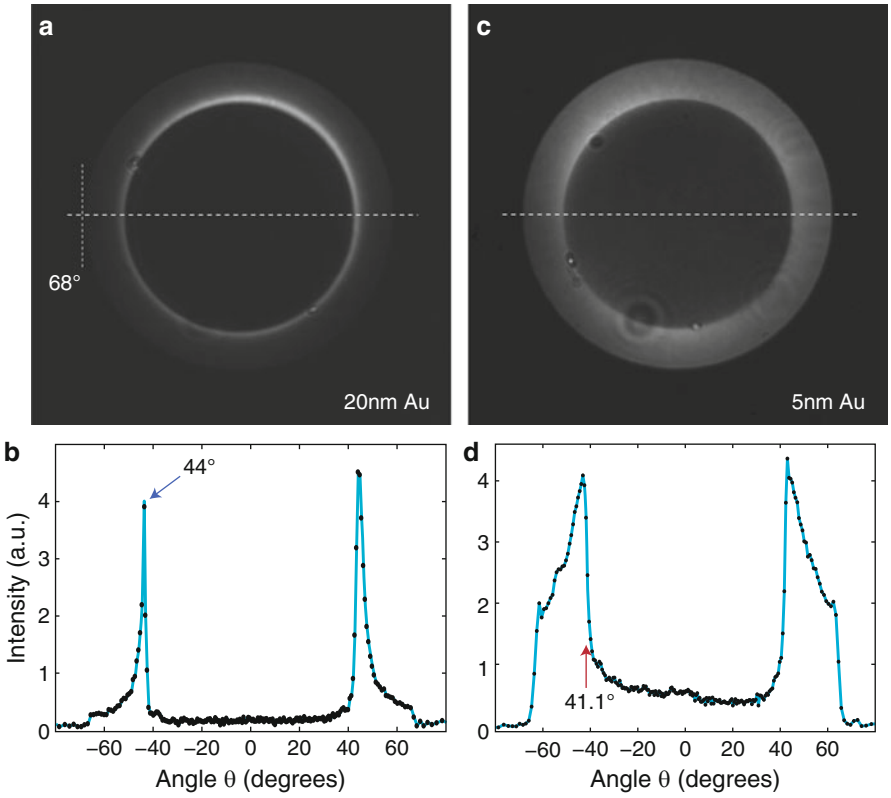


**Fig. 3.6** Fourier plane (FP) imaging of STM-LE light from gold films. (**a**) An FP image for a 20 nm gold film showing a predominant ring centered at $\theta \approx 44°$. (**b**) A cross-section taken along the horizontal *dashed line* in (**a**) confirms that ~80 % of the energy is in the SPP. (**c**) An FP image for a 5 nm gold film featuring a discontinuity at the critical angle $\theta_c = 41°$. (**d**) An intensity cross-section along the *dashed line* in (**c**) shows a random-dipole like emission pattern with a significant fraction of the radiation emitted below the critical angle (denoted by the *arrow*). The maximum angle of collected photons is ~68°, given by the NA of the objective (1.4)

defined crystal facets on the edges. Figure 3.7 shows a real-space optical image of a flake with the gold STM tip positioned at its center with a steady tunneling current. The image shows both a bright central spot along with light scattering from the edges of the flake. Hence, inelastically tunneling electrons can excite gap plasmons which couple to SPPs propagating along the gold flake. The SPPs then scatter at the edges of the flake and give rise to photon emission.

To demonstrate this two-step excitation pathway unambiguously, we next chose to confine the SPP to 1-dimension using a gold nanowire. Monocrystalline nanowires on a similar ITO coated glass substrate were cut to the desired length using a focused gallium ion beam (FIB). The STM tip is placed on one end of the nanowire to generate gap plasmons (and photons). Part of this energy couples to SPPs that then propagate to the other end of the wire where they scatter into photons

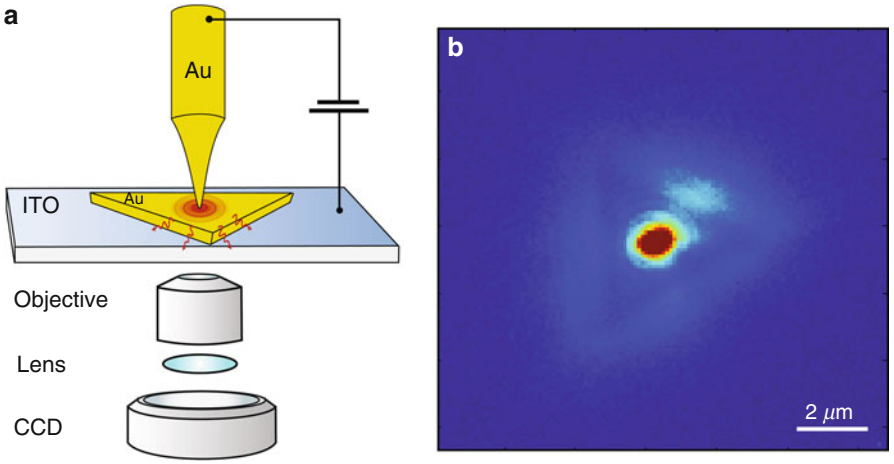


**Fig. 3.7** STM-LE from a monocrystalline gold triangle. (**a**) A schematic of the experiment. The tip is positioned near the middle of the gold flake and a real-space image was acquired by refocusing the emitted photons. (**b**) A real-space image where the contrast arises from the intensity of STM-LE photons. In addition to direct light from the where the tip is placed, there is also scattered radiation coming from the three edges of the flake

(Fig. 3.8). Thus, the nanowire functions as a transmission line mediating between the electrical feed point and the outcoupling region, which in the present case is the hard discontinuity at the far end of the wire.

We have demonstrated that low-energy electrons can couple to photons through a cascade of events that begins with the excitation of a gap plasmon. In the next section, we examine more closely the role of the gap plasmon in STM-LE.

### *3.3.2 Role of the Gap Plasmon in STM-LE*

In order to confirm the role of the gap plasmon in STM-LE, it is necessary to uncover the origin of the line-to-line photoemission intensity variations seen in previous 2-dimensional STM-LE studies [48–52]. These line-to-line variations are typically associated with changes in the probe as it interacts with the sample; however, there have also been reports of electroluminescent (EL) metal clusters being created and/or destroyed within tunnel junctions in a planar geometry [53–55]. We have recently used a series of engineered samples to isolate gap plasmon photoemission from other suspected emissive processes [56].

During a physical tip-sample interaction, in which the tip is physically altered, it is expected that the LSP mode structure of the junction will change as it depends sensitively on the tip geometry [57, 58]. There appear to be physical tip-sample interactions in the STM photoemission and topographic maps on samples composed

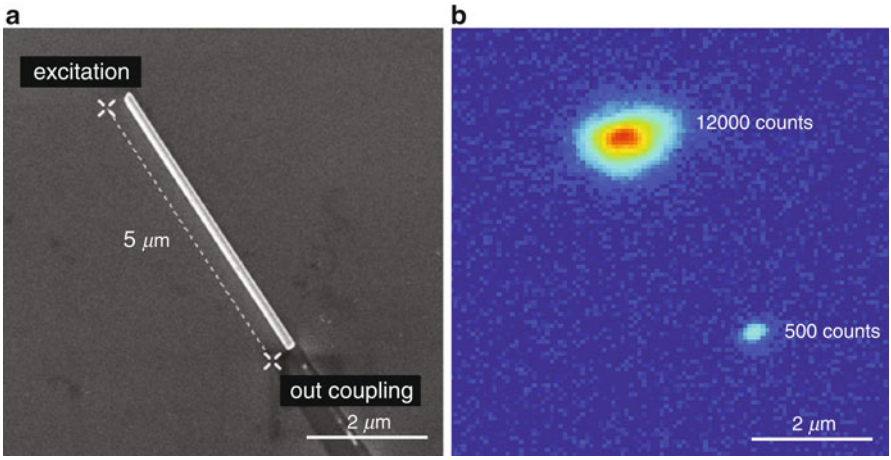


**Fig. 3.8** Electrical excitation of SPPs propagating along a monocrystalline gold nanowire. (**a**) An SEM micrograph of a gold nanowire of radius 87 nm and length ~5 μm. (**b**) A real-space photon emission map obtained by placing the STM tip at one end of the nanowire. SPPs are excited by the STM tip and propagate to the other end of the wire where they are scattered and converted to propagating photons. The wire is immersed in index matching oil to prevent the SPPs from decaying into photons by leakage radiation

of gold particles on a gold film (Fig. 3.9) that could generate or destroy an EL cluster. It is expected that the proximity of a cluster to metal in the tip and sample would lead to significant quenching of electroluminescence, resulting in an emission rate similar to that expected from LSPs alone. Therefore, EL clusters cannot be immediately discounted as a cause of the observed line-to-line emission variations.

One challenge in interpreting the results shown in Fig. 3.9 is that the topographic map obtained with any SPM technique is a convolution between the probe tip geometry and the true sample topography; this convolution can have significant effects on the topographic map [59, 60]. For STM-LE studies, it is important to note that the LSP closely links the photoemission map with the topographic map. In general, larger sample excursions lead to increased sampling of the tip area during the convolution process. Since the mode structure of the LSPs depend on the tip shape, and since different areas of the tip are being sampled by a single topographic feature, the conclusions drawn from STM-LE on high-topography samples can be suspect.

The effects of the tip convolution on the data can be minimized by constructing ultra-flat samples. If the sample has no topographic excursions present to sample the probe then only a specific, and ideally unchanging, part of the probe will take part in the tunneling process. The technique of template-stripping has recently been extended beyond metallic samples to create ultra-smooth samples composed of metals, semiconductors, and/or oxides [61]. We have created specially structured, ultra-flat samples to study STM-LE in a controlled manner [56]. These samples consisted of triangular gold patches, with a side length of 50 nm, surrounded by a 3 nm platinum film.

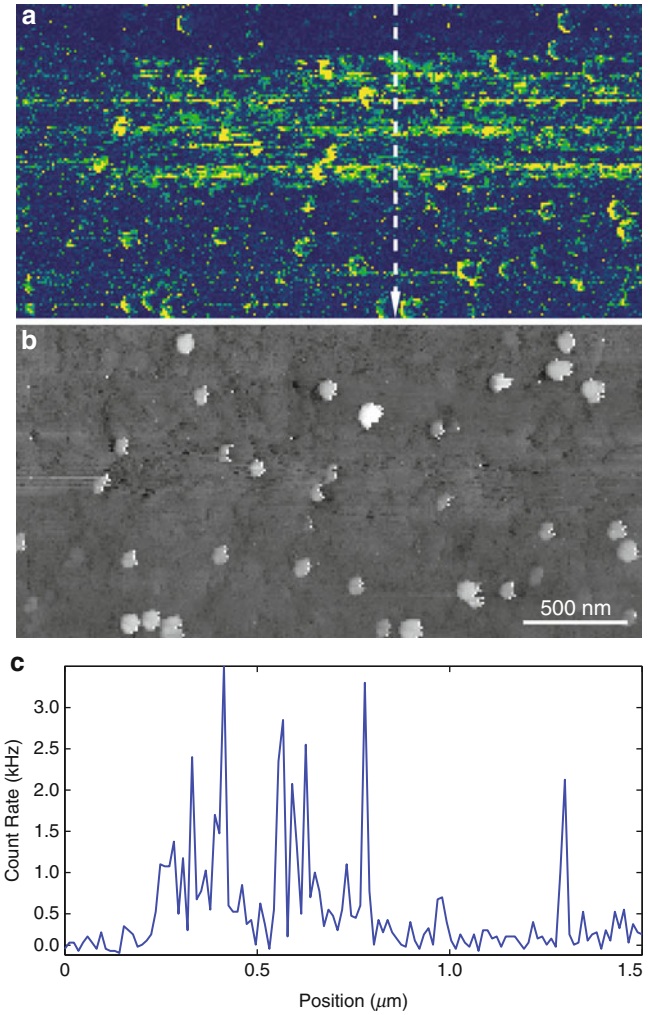


**Fig. 3.9** (**a**) An STM-LE map of a sample composed of 30 nm diameter gold particles deposited on a 20 nm thick gold film and (**b**) the corresponding topographic map. (**c**) A cross-section along the *dashed line* in (**a**). Significant line-to-line photoemission variations are seen along with enhanced emission at the particle edges. (STM parameters: $V_s$ = 2.0 V, I = 1.0 nA)

Two specific properties of the metals, as well as their close proximity, allow for the differentiation between emission from an EL cluster and from an LSP. First, gold and platinum have similar work functions and it is therefore expected that the tunneling barrier associated with an STM would have a similar height and width on both materials. A constant tunneling barrier is expected to lead to similar EL output on both materials. Second, the imaginary part of the dielectric function

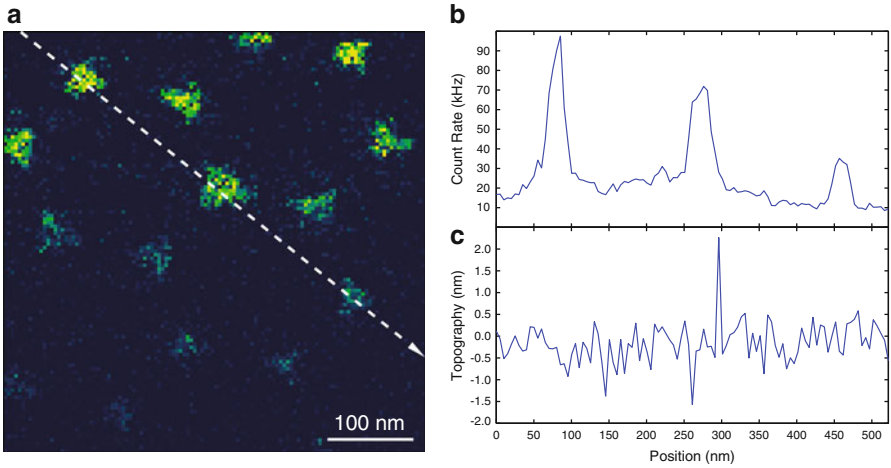


**Fig. 3.10** (**a**) An STM-LE map of a low-roughness sample composed of gold triangles embedded in a platinum matrix. (**b**) A smoothed cross-section along the *dashed line* in (**a**) and (**c**) the corresponding raw topographic cross-section. The RMS roughness of the topography shown in (**c**) is ∼450 pm. Photoemission is observed to vary line-to-line; however, the ratio of emission rates between gold and platinum remains constant (STM parameters: $V_s = 2.1$ V, I = 0.7 nA)

of platinum is more than an order of magnitude larger than that of gold in the typical STM-LE band near $\lambda = 700$ nm. It is expected that the plasmonic activity on platinum is greatly quenched in comparison to gold due to higher non-radiative plasmonic energy losses in platinum.

A photoemission map generated on such a sample is shown in Fig. 3.10a. Topography confirms that the sample is very flat (Fig. 3.10c) and it is therefore expected to be free of artifacts associated with a tip-sample convolution. In fact, extremely fine (less than 10 nm) features, such as the corners of the gold triangles, are resolvable and this resolution is independent of the tip radius. The photoemission rate varies from line-to-line and greatly depends on sample material. The gold triangles clearly give a larger emission rate than the platinum film. While the emission rate varies between lines, the ratio of emission rates between the gold and platinum remains constant as shown in Fig. 3.10b. This type of sample was studied by systematically varying the sample bias voltage, bias polarity, and set-point current as well as performing the study with multiple tips and samples. The emission behavior remained qualitatively the same in each case. These experiments indicate that EL clusters are rare or non-existent in STM tunnel junctions.

We additionally fabricated a complimentary sample to confirm that EL clusters were not present in STM-LE experiments. In this case, the sample consisted of gold patterns deposited onto ITO. Since LSPs cannot exist on ITO with energies in the 2 eV range, the emission of light on ITO from an STM junction would indicate the presence of an EL cluster. A representative example of a photoemission map on this type of sample is shown in Fig. 3.11a. No light appears to be emitted on the

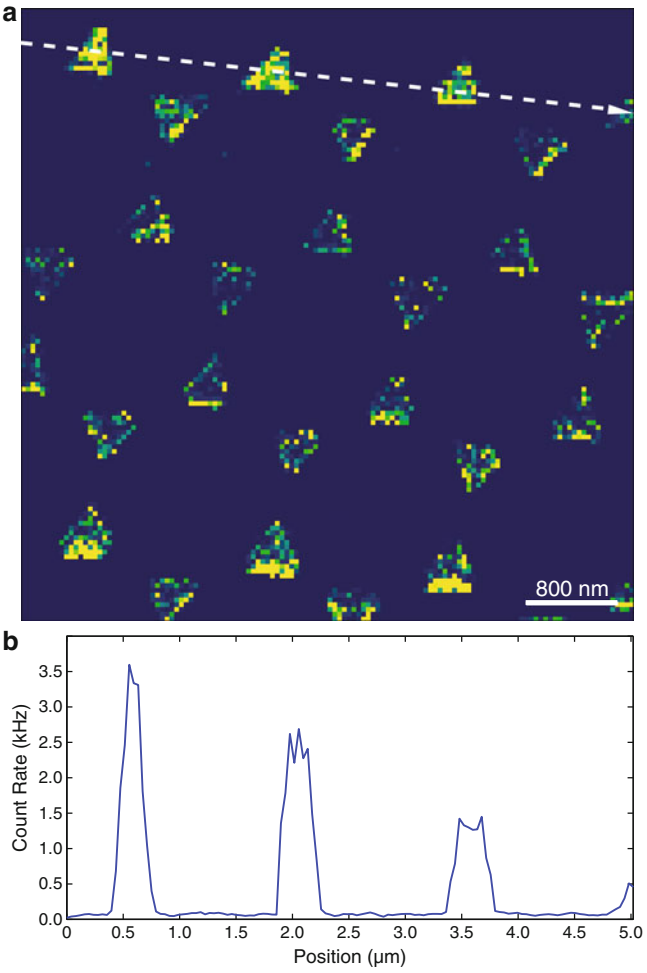


**Fig. 3.11** (**a**) An STM-LE map of a sample composed of 20 nm thick gold triangular patterns deposited on a 150 nm thick ITO film on a glass substrate. (**b**) A cross-section along the *dashed line* in (**a**). Photoemission is only observed from the gold surfaces (STM parameters: $V_s = 2.25$ V, I = 0.2 nA)

ITO film at any time. The light emission rate varies greatly between lines but the emission regions are strictly confined to the gold triangles as shown in Fig. 3.11b. Again, the emission behavior of this type of sample remained qualitatively the same as experimental parameters were systematically varied.

We can draw two conclusions from these results. First, EL clusters do not appear to be a significant source of light from an STM. Second, the LSP mode structure is greatly affected not only by physical changes in the tip due to interactions with the sample but also by the sample material and topography. The variation in emission

rates shown in Fig. 3.9a can be explained in these terms. The line-to-line variations shown are due to tip-sample interactions which lead to a spatially varying LSP mode structure. Also, as the probe approaches close to a particle, the tunnel junction is reoriented and exists between the side of the particle and the side of the probe. This reorientation, from vertical to horizontal, of the LSP modes explains the apparent rings of photoemission around the particles.

### *3.3.3 Concluding Remarks on STM-LE*

Electron tunneling provides a non-optical, voltage-controlled, low energy, and nanoscale pathway for launching SPPs in nanostructures. It is important to point out the advantages of this technique over related schemes. Previous work has been done under vacuum with high energy elections which is not practical for on-chip implementation. Additionally, exciton-mediated approaches using inorganic or organic semiconductors require multi-step fabrication which increases device complexity. The method introduced here only requires metal electrodes that can be easily integrated in a planar geometry.

The study of electrically excited SPPs can be extended to separately optimize the electron-plasmon and plasmon-photon coupling strengths. This can be expected to result in an increase in the overall efficiency of the process from $\sim 10^{-5}$ presently to a level where it can be of technological relevance. In addition to propagating SPPs, low energy electrons can also be used to excite localized plasmon modes in nanostructures, which can then be coupled optical antennas. It is conceivable that the electrical excitation scheme can be applied to highly directional antennas, such as Yagi-Uda antennas, enabling a direct conversion of low energy electrons to a directed beam of far-field photons.

**Acknowledgements** We are grateful for financial support by the Swiss National Science Foundation (grant 200021_149433).

## References

1. Abbe E (1873) Beiträge zur Theorie des Mikroskops und der mikroskopischen Wahrnehmung. Archiv f Mikroskop Anat 9:413
2. Rayleigh L (1896) On the theory of optical images with special reference to the optical microscope. Phil Mag 5(42):167–195
3. Bharadwaj P, Deutsch B, Novotny L (2009) Optical antennas. Adv Opt Phot 1:438–483
4. Xie XS, Trautman JK (1998) Optical studies of single molecules at room temperature. Annu Rev Phys Chem 49:441–480
5. Specht M, Pedarning JD, Heckl WM, Hänsch TW (1992) Scanning plasmon near-field microscope. Phys Rev Lett 68:476–479
6. Xia Y (2005) Shape-controlled synthesis and surface plasmonic properties of metallic nanostructures. MRS Bull 30:338

7. Höppener C, Novotny L (2008) Antenna-based optical imaging of single $Ca^{2+}$ transmembrane proteins in liquids. Nano Lett 8:642–646
8. Höppener C, Beams R, Novotny L (2009) Background suppression in near-field optical imaging. Nano Lett 9:903–908
9. Lapin ZJ, Christiane H, Gelbard HA, Lukas N (2012) Near-field quantification of complement receptor 1 (cr1/cd35) protein clustering in human erythrocytes. J Neuroimmune Pharmacol 7(3):539–543
10. Anger P, Bharadwaj P, Novotny L (2006) Enhancement and quenching of single molecule fluorescence. Phys Rev Lett 96:113002
11. Bharadwaj P, Beams R, Novotny L (2011) Nanoscale spectroscopy with optical antennas. Chem Sci 2:136–140
12. Ichimura T, Hayazawa N, Hashimoto M, Inouye Y, Kawata S (2004) Tip-enhanced coherent anti-stokes Raman scattering for vibrational nanoimaging. Phys Rev Lett 92:2004
13. Cançado LG, Hartschuh A, Novotny L (2009) Tip enhanced Raman scattering of carbon nanotubes. J Raman Spectrosc 40:1420–1426
14. Johnson TW, Lapin ZJ, Ryan B, Lindquist NC, Rodrigo SG, Lukas N, Sang-Hyun O (2012) Highly reproducible near-field optical imaging with sub-20-nm resolution based on template-stripped gold pyramids. ACS Nano 6(10):9168–9174
15. Palomba S, Danckwerts M, Novotny L (2009) Nonlinear plasmonics with gold nanoparticle antennas. J Opt A Pure Appl Opt 11:114030
16. Deutsch B, Hillenbrand R, Novotny L (2010) Visualizing the optical interaction tensor of a gold nanoparticle pair. Nano Lett 10:652–656
17. Deutsch B, Hillenbrand R, Novotny L (2008) Near-field amplitude and phase recovery using phase-shifting interferometry. Opt Express 16:494–501
18. Schnell M, Garcia-Etxarri A, Huber AJ, Crozier KB, Borisov A, Aizpurua J, Hillenbrand R (2010) Amplitude- and phase-resolved near-field mapping of infrared antenna modes by transmission-mode scattering-type near-field microscopy. J Phys Chem C 114(16):7341–7345
19. Stiegler JM, Abate Y, Cvitkovic A, Romanyuk YE, Huber AJ, Leone SR, Hillenbrand R (2011) Nanoscale infrared absorption spectroscopy of individual nanoparticles enabled by scattering-type near-field microscopy. ACS Nano 5(8):6494–6499
20. Novotny L (2007) The history of near-field optics. Prog Opt 50:137–180
21. McMullan D (1990) The prehistory of scanned image microscopy. Part I: scanned optical microscopes. Proc Roy Microsc Soc 25(2):127–131
22. Pohl DW (2004) Optics at the nanometre scale. Phil Trans R Soc Lond A 362:701–717
23. Binnig G, Rohrer H, Gerber C, Weibel E (1982) Tunneling through a controllable vacuum gap. Appl Phys Lett 40:178–180
24. Binnig G, Rohrer H (1982) Scanning tunneling microscopy. Helv Phys Acta 55:726
25. Binnig G, Quate CF, Gerber C (1986) Atomic force microscope. Phys Rev Lett 56:930
26. Pohl DW, Denk W, Lanz M (1984) Optical stethoscopy: image recording with resolution l=20. Appl Phys Lett 44:651–653
27. Fischer UC, Pohl DW (1989) Observation on single-particle plasmons by near-field optical microscopy. Phys Rev Lett 62:458–461
28. Novotny L (2007) Effective wavelength scaling for optical antennas. Phys Rev Lett 98:266802
29. Kalkbrenner T, Ramstein M, Mlynek J, Sandoghdar V (2001) A single gold particle as a probe for apertureless scanning near-field optical microscopy. J Microsc 202:72–76
30. Christiane H, Zachary L, Palash B, Lukas N (2012) Self-similar gold-nanoparticle antennas for a cascaded enhancement of the optical field. Phys Rev Lett 109(1):017402
31. Novotny L, Bian RX, Xie XS (1997) Theory of nanometric optical tweezers. Phys Rev Lett 79:645–648
32. Novotny L, Sanchez EJ, Xie XS (1998) Near-field optical imaging using metal tips illuminated by higher-order Hermite-Gaussian beams. Ultramicroscopy 71:21–29
33. Ritchie RH (1957) Plasma losses by fast electrons in thin films. Phys Rev 106:874–881
34. Räther H (1965) Solid state excitations by electrons. In: Springer tracts in modern physics, vol 38. Springer, Berlin, pp 84–157

35. Bashevoy MV, Jonsson F, Krasavin AV, Zheludev NI, Chen Y, Stockman MI (2006) Generation of traveling surface plasmon waves by free-electron impact. Nano Lett 6:1113–1115
36. Vesseur EJR, de Waele R, Kuttge M, Polman A (2007) Direct observation of plasmonic modes in au nanowires using high-resolution cathodoluminescence spectroscopy. Nano Lett 7: 2843–2846
37. Cai W, Sainidou R, Xu J, Polman A, Garcia de Abajo FJ (2009) Efficient generation of propagating plasmons by electron beams. Nano Lett 9:1176–1181
38. Jaysen N, Mathieu K, Stéphan O, García de Abajo FJ, Tencé M, Henrard L, Taverna D, Pastoriza-Santos I, Liz-Marzán LM, Colliex C (2007) Mapping surface plasmons on a single metallic nanoparticle. Nat Phys 3:348–353
39. Kuttge M, Vesseur EJR, Polman A (2009) Fabry-Pérot resonators for surface plasmon polaritons probed by cathodoluminescence. Appl Phys Lett 94:183104
40. Lambe J, McCarthy SL (1976) Light emission from inelastic electron tunneling. Phys Rev Lett 37:923
41. Gimzewski JK, Reihl B, Coombs JH, Schlittler RR (1988) Photon emission with the scanning tunneling microscope. Z Phys B 72:497–501
42. Coombs J, Gimzewski J, Reihl B, Sass J (1988) Photon emission experiments with the scanning tunnelling microscope. J Microsc 152:325–336
43. Johansson P, Monreal R, Peter A (1990) Theory for light emission from a scanning tunneling microscope. Phys Rev B 42:9210–9213
44. Berndt R, Gimzewski JK, Johansson P (1991) Inelastic tunneling excitation of tip-induced plasmon modes on noble-metal surfaces. Phys Rev Lett 67:3796–3799
45. Uehara Y, Kimura Y, Ushioda S, Takeuchi K (1992) Theory of visible light emission from scanning tunneling microscope. Jpn J Appl Phys 31:2465–2469
46. Takeuchi K, Uehara Y, Ushioda S, Morita S (1991) Prism? Coupled light emission from a scanning tunneling microscope. J Vac Sci Technol B 9:557–560
47. Bharadwaj P, Novotny L (2011) Robustness of quantum dot power-law blinking. Nano Lett 11:2137–2141
48. Walmsley DG, Tan T-S, Dawson P (2004) Light emission from gold and silver thin films in a scanning tunneling microscope: role of contamination and interpretation of grain structure in photon maps. Surf Sci 572(23):497–520
49. Silly F, Gusev AO, Taleb A, Pileni M-P, Charra F (2002) Single nanoparticle manipulation with simultaneously recorded stm-induced light emission. Mater Sci Eng C 19(12):193–195
50. Perronet K, Barbier L, Charra F (2004) Influence of the Au(111) reconstruction on the light emission induced by a scanning tunneling microscope. Phys Rev B 70:201405
51. Uemura T, Akai-Kasaya M, Saito A, Aono M, Kuwahara Y (2008) Spatially resolved detection of plasmon-enhanced fluorescence using scanning tunneling microscopy. Surf Interface Anal 40(6-7):1050–1053
52. Fujita D, Onishi K, Niori N (2004) Light emission induced by tunneling electrons from surface nanostructures observed by novel conductive and transparent probes. Microsc Res Tech 64(5–6):403–414
53. Gonzalez JI, Lee T-H, Barnes MD, Antoku Y, Dickson RM (2004) Quantum mechanical single-gold-nanocluster electroluminescent light source at room temperature. Phys Rev Lett 93:147402
54. Tae-Hee L, Gonzalez JI, Dickson RM (2002) Strongly enhanced field-dependent single-molecule electroluminescence. Proc Natl Acad Sci U S A 99(16):10272–10275
55. Tae-Hee L, Dickson RM (2003) Single-molecule leds from nanoscale electroluminescent junctions. J Phys Chem B 107(30):7387–7390
56. Divitt S, Bharadwaj P, Novotny L (2013) The role of gap plasmons in light emission from tunnel junctions. Opt Express 21(22):27452–27459
57. Mitra J, Lei F, Boyle MG, Dawson P (2009) Electromagnetic interaction between a metallic nanoparticle and surface in tunnelling proximitymodelling and experiment. J Phys D Appl Phys 42(21):215101

58. Boyle MG, Mitra J, Dawson P (2009) Infrared emission from tunneling electrons: the end of the rainbow in scanning tunneling microscopy. Appl Phys Lett 94(23):233118
59. Dawson P, Boyle MG (2006) Light emission from scanning tunnelling microscope on polycrystalline Au films? What is happening at the single-grain level? J Opt A Pure Appl Opt 8:S219
60. Branscheid R, Jacobsen V, Kreiter M (2007) STM induced light from nontrivial metal structures: local variations in emission efficiency. Surf Sci 602:176
61. Park JH, Nagpal P, McPeak KM, Lindquist NC, Oh S-H, Norris DJ (2013) Fabrication of smooth patterned structures of refractory metals, semiconductors, and oxides via template stripping. ACS Appl Mater Interfaces 5(19):9701–9708